RESEARCH ARTICLE | FEBRUARY 12 2025

Data-driven deep learning models in particle-laden turbulent flow

Special Collection: Recent Advances in Fluid Dynamics and Its Applications

R. Hassanian ; Á. Helgadóttir ; F. Gharibi ; A. Beck ; M. Riedel

Physics of Fluids 37, 023348 (2025)
https://doi.org/10.1063/5.0251765

Physics of Fluids ARTICLE pubs.aip.org/aip/pof

Data-driven deep learning models in particle-laden turbulent flow

Cite as: Phys. Fluids **37**, 023348 (2025); doi: 10.1063/5.0251765
Submitted: 4 December 2024 · Accepted: 17 January 2025 ·
Published Online: 12 February 2025

R. Hassanian,[1,a)] Á. Helgadóttir,[1] F. Gharibi,[2] A. Beck,[3] and M. Riedel[1,4]

AFFILIATIONS

[1]Faculty of Industrial Engineering, Mechanical Engineering, and Computer Science, University of Iceland, 102 Reykjavík, Iceland
[2]Laboratory of Fluid Dynamics and Technical Flows, Otto-von-Guericke University of Magdeburg, 39106 Magdeburg, Germany
[3]Institute of Aerodynamics and Gas Dynamics, University of Stuttgart, 70563 Stuttgart, Germany
[4]Juelich Supercomputing Centre, 52428 Jülich, Germany

Note: This paper is part of the Special Topic, Recent Advances in Fluid Dynamics and Its Applications.
[a)]**Author to whom correspondence should be addressed:** seh@hi.is

ABSTRACT

The dynamics of inertial particles in turbulent flow are complex, and in practice, gravity influences particle dynamics. However, the effects of gravity have not been appropriately investigated using numerical approaches. This study provides the first empirical evidence of a data-driven deep learning (DL) model to predict the velocity, displacement, and acceleration of inertial particles in a strained particle-laden turbulent flow. This study introduces a DL model to experimental data from Hassanian *et al.*, who investigated distorted turbulent flow within a specific range of Taylor microscale Reynolds number, $100 < Re_\lambda < 120$. The flow experienced a vertical mean strain rate of 8 s^{-1} under the influence of gravity. Lagrangian particle tracking technique was employed to capture each inertial particle's velocity field and displacement. The deep learning model relies on experimental particle-laden turbulent flow, demonstrating all effective parameters, including turbulence intensity, strain rate, turbulent energy dissipation rate, gravity, particle size, particle density, and small and large-scale effects. The forecasting model demonstrates significant capability and high accuracy in generating predictions closely aligned with the actual data. Model training and inference are run on the high-performance computing DEEP-DAM system at the Jülich Supercomputing Center. The proposed approach can potentially enhance the understanding of inertial particle dynamics and the parameters that affect them. Furthermore, data-driven models can offer new insights into particle motion and the underlying differential equations within physics-based deep learning frameworks.

I. INTRODUCTION

Particle-laden turbulent (PLT) flows are observed across various scales and environments.[1] In the natural world, examples include dust storms, sandstorms, volcanic ash clouds, oceanic sediment transport,[2] cloud formation, glacial outwash, and sediment transport in rivers.[3] Industrial applications relying on PLT flows include spray drying, cyclone separators, pneumatic conveying systems, combustion processes, paint spraying and powder coating, pharmaceutical granulation and mixing, mining and mineral processing,[4] and erosion prediction for jet engines in aerospace engineering.[5] In biological fluid dynamics, examples of PLT flows include the deposition of inhaled aerosols in respiratory tracts,[6] as well as blood flow and clot formation.[7]

All the cases mentioned are fundamentally linked by the physics of multiphase flow.[8] PLT flows involve two distinct phases: a continuous fluid phase and a dispersed particulate phase. The complexity of PLT flows stems not only from the intrinsic challenges of turbulent flow—an enduring unsolved problem in physics[2,9]—but also from the intricate interactions between the fluid and particulate phases.[4,10] These interactions encompass the exchange of energy, momentum, and mass.

PLT flows are classified according to the nature of interactions between the phases, which is defined based on the particle volume fraction term (Φ_p) for the interaction ranges.[10] When $\Phi_p < 10^{-6}$, the effect of particles on turbulence is negligible, and the flow is termed one-way coupled. For $10^{-6} < \Phi_p < 10^{-3}$, the flow is classified as two-way coupled, where the momentum transfer from particles to the turbulent flow becomes significant. In the third category, $\Phi_p > 10^{-3}$, there is both two-way particle–turbulence interaction and particle–particle collisions, making it four-way coupled. As Φ_p approaches 1, the flow transitions to a granular flow, as the fluid phase becomes negligible.[10]

In one-way coupled PLT flow, particle behavior is relatively well understood, particularly in unbounded homogeneous turbulent flows. However, the primary challenge lies in the incomplete understanding of turbulent flow itself.[11] For two-way and four-way coupled PLT flows, the high nonlinearity of interactions places them at an early stage of scientific comprehension.[12] Advancing our understanding of these interactions could enhance predictions of the complex dynamics and behavior of particles. In continuous turbulent flow, which is characterized by fluctuations in velocity and pressure across space and time, the PLT flow introduces an additional factor: the dispersed phase, exhibiting a random, time-dependent distribution and movement of particles.[13] Moreover, while the smallest length scale in turbulent flow corresponds to the Kolmogorov scale, PLT flow also incorporates the particle scale as a critical consideration.[14]

There are three primary numerical approaches to studying PLT flow: mathematical methods using closure models, direct numerical simulations (DNS) of PLT flows, and large eddy simulation (LES).[15–17] These studies emphasize the limitations and essential preliminary steps required to advance the understanding of PLT flow.[10] Turbulence closure models for particle-laden flows are especially critical, as a comprehensive understanding of the complex physics governing the interaction between turbulence and dispersed particles is essential.[10] Notable limitations exist in the particle motion (Maxey–Riley) equation,[18] which adopts a Lagrangian perspective. Taylor's theory of turbulent diffusion,[19] originally formulated for fluid points, is only directly applicable to solid particles in a zero-gravity environment, with significant deviations observed under the influence of gravity. In zero gravity, the inertia of a solid particle may lead to turbulent diffusivity surpassing that of a fluid point. However, under gravitational conditions, the turbulent diffusivity of solid particles diminishes due to the combined effects of inertia and gravity.[10,20]

Analyzing the forces acting on a solid particle over time reveals that in the gravitational direction, buoyancy and drag forces predominantly govern particle behavior, with buoyancy occasionally surpassing drag.[10,21] In the lateral directions, drag and Basset forces play a key role, although drag is typically at least an order of magnitude greater than the Basset force.[22] In the homogeneous, two-way coupled PLT flow, particles enhance the fluid's turbulent energy at high wave numbers. However, in the absence of external drivers such as shear or buoyancy, this turbulent energy dissipates more quickly than in turbulence without particles. Under gravitational conditions, particles transfer their momentum to small-scale motion in an anisotropic manner.[4,10]

Despite its limitations and challenges, DNS[23] provides valuable insights into the fine structure of turbulence, particle dispersion, and two-way particle-turbulence interactions at moderate Reynolds numbers (Re_l). In DNS, the computational cost of resolving a single dependent variable[23] (e.g., a variable component capturing the spatial and temporal behavior of a large eddy) scales as R_l^3. For most engineering applications, Re_l is typically around 10^3, for aerospace applications, it is at least 10^5, while for geophysical flows, Re_l can reach approximately 10^8. These computational demands are further exacerbated by the inclusion of dispersed particles, making DNS extremely resource-intensive, even with advancements in high-performance computing and the advent of Exascale capabilities.[10]

A critical issue is that gravity is often excluded from PLT flow simulations, as its inclusion substantially increases computational requirements.[24] Most studies focus on fundamental particle-turbulence interactions, treating gravity as a known linear force. In many high-speed turbulent flows, particularly in gases, inertial and turbulent forces dominate gravitational forces.[25] However, it is recognized that zero-gravity results cannot always be extended to gravity environments,[25] as the effects of gravity on these interactions are not yet fully understood.

Considering the limitations of current numerical techniques and the need for methods to address specific challenges, deep learning (DL) approaches hold promise in this field.[26,27] Data-driven models (DDMs) align with the core philosophy of the emerging hybrid analysis and modeling (HAM) paradigm.[28] HAM optimally combines physics-based models (PBMs) with data-driven models to capture unmodeled or unknown physical phenomena. DDMs do not rely on theoretical equations but instead derive insights from data correlations.[29] Recognizing the correlations between training variables and target variables is essential in a DDM. Hassanian *et al.*[30] applied DDM to predict the velocity of turbulent flow based on tracer particles representative of the flow stream. Among sequential DL models, long-short term memory (LSTM), gated recurrent unit (GRU),[31] convolutional neural networks (CNN) and transformer[32,33] display a remarkable ability to predict nonlinear and high dimensional phenomenon such as turbulent flow. Hassanian *et al.*[31,32,34] established a framework that defines the connection between Lagrangian perspectives on turbulent flow properties and sequential models such as LSTM, GRU, and transformer. This framework has the potential to be extended to inertial particles within the Lagrangian framework and serves as the foundation for the present study.[32] A neural network interpolation (NNI) was developed to enhance the prediction of preferential concentration in simulations of PLT flow by Hu *et al.*[35] Encoder–decoder, U-Net, generative adversarial network (GAN) models are compared to predict the particles in two-dimensional turbulence based on data from DNS by Maruel *et al.*[36] Groll *et al.*[37] used deep neural network models to predict particle-laden pipe flows based on LES data. Barigou *et al.*[38] applied a hybrid machine-learning algorithm to analyze turbulent particle transport in a horizontal pipe for experimental data.

The motivation for this study is to apply data-driven models (DDMs) to experimental data on PLT undergoing a strain deformation and evaluate the capability of DL models in predicting particle dynamics. The superiority of the current study is that it applies the DL model for PLT experimental data. This approach aims to support future analyses of particle–turbulence eddy interactions, particle-particle interactions, and the effects of gravity. The model was trained on data from laboratory measurements conducted by Hassanian *et al.*[3] The experiments were performed multiple times, first with tracer particles to characterize the turbulent flow and then with inertial particles to record attributes such as position and velocity and calculate the acceleration.

Lagrangian particle tracking (LPT) was used for measurements, focusing on the dynamics of solid particles in an incompressible flow. The experimental setup represented a realistic environment, simulating three-dimensional flow and including gravitational effects. Measurements were conducted in 2D, recording two components of the flow properties. A GRU model was designed and utilized to predict inertial particle displacement, velocity, and acceleration. In order to have enough data in training, the flow use case was repeated five times, and the model was with a split of train-test equal to 80%–20%. This approach could assist in integrating DDM to PBM for PLT flow.

Furthermore, developing such a model could enhance explainable DL models to investigate the physical properties and the influences in PLT flow. Hence, this paper is organized as follows: Sec. II presents the applied method and theory, and Sec. III explains the DL architecture and data-model tuning. Section IV presents the results and discussion, and Sec. V provides the conclusion.

II. THEORY AND METHODOLOGY

This study proposes a novel approach employing the gated recurrent unit (GRU) model to predict inertial particle movement in strained PLT flow from the experiment,[3] enhancing DL application in PLT. The applied theory and the details of the data setup are explained in the following subsections.

A. Theory

In order to apply DDM for PLT, data from such a flow is required, which could come from LES, DNS, or experimental data. According to the above-mentioned matters in numerical approaches, using measured data from experiments is an excellent choice since it covers the real environment and influences and this is the novelty and robustness of the current study. Based on the Lagrangian viewpoint, one can track a particle in turbulent flow and extract the properties such as displacement, velocity, and acceleration over time. Thus, via the Lagrangian viewpoint, displacement and instantaneous velocity for a single particle are defined as follows:[2]

$$x_{p,i} = x_{p,i}(t, x_{i,0}), \tag{1}$$

$$U_{p,i} = U_{p,i}(t, x_1(t, x_{1,0}), x_2(t, x_{2,0}), x_3(t, x_{3,0})), \tag{2}$$

where the fluid particle position and velocity in 3D coordinates are determined by notations 1 and 2, respectively, x_p is the position, U_p is the instantaneous velocity, t is the time, and i specifies the vector component. In this work, data were measured in 2D; therefore, the third dimension has not been addressed. In the Lagrangian perspective, instantaneous particle acceleration can be defined as

$$a_{p,i} = \frac{dU_{p,i}}{dt}, \tag{3}$$

where a_p is instantaneous acceleration of a particle. The instantaneous acceleration of a particle in turbulent flow from the Lagrangian viewpoint is generally written based on Maxey–Riley equation[10,18]

$$\begin{aligned}\frac{dU_{p,i}}{dt} = {} & \frac{u_{f,i} - U_{p,i}}{\tau_p} + \frac{m_f}{m_p}\frac{Du_{f,i}}{Dt} + \frac{1}{2}\frac{m_f}{m_p}\left(\frac{Du_{f,i}}{Dt} - \frac{dU_{p,i}}{dt}\right) \\ & + \frac{6a^2(\pi\rho\mu)^{1/2}}{m_p}\int_{\tau_{p0}}^{\tau_p}\frac{d(u_{f,i} - U_{p,i})/d\tau}{(t_p - \tau)^{1/2}}\,d\tau \\ & + \left(1 - \frac{m_f}{m_p}\right)g_i + \frac{1}{2}\frac{(\pi\rho a^2)}{m_p}C_L L_i V^2,\end{aligned} \tag{4}$$

where it describes the balance of forces acting on the particle (sphere) as it moves along its trajectory. In Eq. (4), u_f is the flow velocity, τ_p is the particle response time, m_p is the mass of the particle, m_f is the mass of the fluid displaced by the particle, a is the particle (sphere) radius, ρ is the uniform density of incompressible fluid, μ is the dynamic viscosity, g is the gravity acceleration, d/dt denotes a time derivative following the moving particle, and D/Dt denotes a Lagrangian time derivative following a fluid element. The term on the left-hand side is the inertia force acting on the particle due to its acceleration. The terms on the right side are, respectively the forces due to viscous and pressure drag, fluid pressure gradient and viscous stresses, inertia of virtual mass, viscous drag due to unsteady relative acceleration (Basset),[39,40] buoyancy, and Saffman's lift force due to shear in the carrier flow.[41,42] C_L is the lift coefficient evaluated by Saffman; L_i are the three x_i direction cosines; and V is the magnitude of the relative velocity vector. It should be mentioned here that this form of Saffman's lift force is quite restricted by the condition that $Rs \ll R_g^{1/2}$, where $R_s = v_r d/\mu$ and $R_g = Gd^2/\mu$; G is the gradient of fluid velocity, d is the sphere diameter, and v_r is the slip velocity. Later, McLaughlin[43] and more recently, Shi and Rzehak[44] removed the restrictions of the lift force term and estimated it numerically.[45]

The aforementioned instantaneous acceleration of the inertial particle involves certain numerical estimations and limitations. The current study proposes utilizing the DDM model to predict the acceleration without referred estimations. Furthermore, the effect of the gravitational environment can be examined by contrasting it with Eq. (4), where the gravitational term is disabled.

B. Particle measured data

This study applies measured displacement, velocity, and acceleration of solid glass inertial particles with diameters of 210–250 μm and a density of 2.1 g/cm^3 to develop a DL model prediction for inertial particles in PLT flow. The experiment was performed in a tank with dimensions of $60 \times 60 \times 60$ cm^3, and the measurement area was located at the center of the tank, with dimensions of 24.5×24.5 mm^2. The flow was initially nearly homogeneous and isotropic, undergoing strain deformation at 8 s^{-1} in the y-direction (vertical). Figure 1 presents a schematic representation illustrating three frames from the experiment. It shows how the strain deformation, generated by the nearly uniform movement of two circular disks toward the center of the tank, causes the particles to distribute and move within the deformed turbulent flow of the fluid (water). The straining PLT flow is a use case that can observed in many artificial and natural events. Airborne flow approaches the leading edge of the wind turbine,[46] and dust flow hits petrochemical turbo machines blades,[8] stagnation point,[20] particle interaction in mixing chamber far from the walls, and internal flow in a changeable cross section are instances.[2,3] Prior to conducting experiments with inertial particles, turbulent flow was generated in the range of Taylor microscale Reynolds numbers, $100 < Re_\lambda < 120$, using the PIV technique and tracer particles (hollow glass spheres with diameters of 80–100 μm and a density of 1.1 g/cm^3). Measurements were taken from the flow before the strain deformation to calculate the Reynolds and Stokes numbers. The Stokes number for inertial particles ranged from 0.113 to 0.161. The Kolmogorov length and time scales were 0.177 mm and 31.6 ms, respectively. It is important to note that once the turbulent flow underwent strain deformation, the Stokes number could change relative to its initial value. However, it can be reasonably assumed that the particles remained in the inertial regime. Additionally, the turbulent dissipation rate was measured within the inertial subrange, where it maintained an approximately constant value.

The Lagrangian particle tracking (LPT) technique is employed to identify individual and extended particle trajectories. This study does

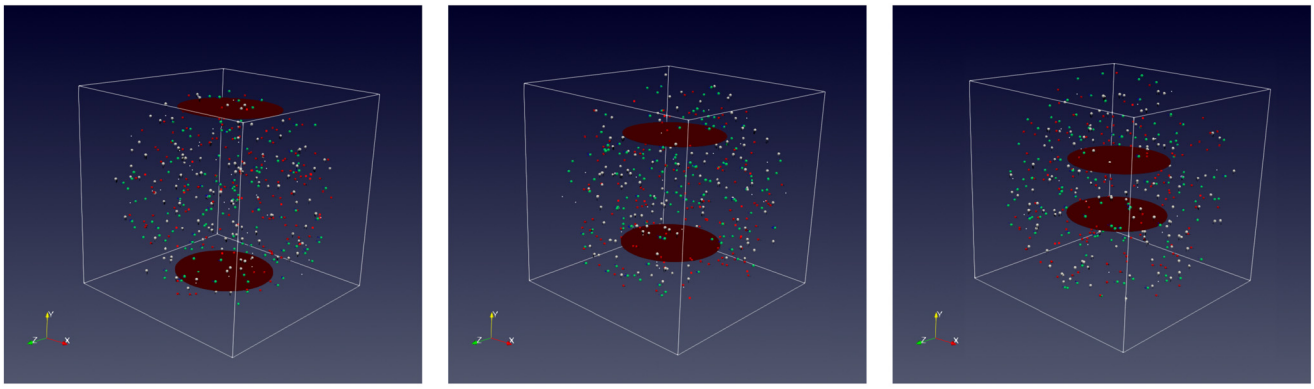

(a) Frame 1 (b) Frame 2 (c) Frame 3

FIG. 1. A schematic representation of three strained particle-laden turbulent flow frames. Particles with different colors illustrate different movement directions for inertial particles. Two red circular disks, positioned at the top and bottom of the tank, move toward the center, generating strain deformation.

not involve new empirical work but instead utilizes data from previously validated laboratory experiments. Details of the experimental setup and procedure are provided in the original work.[3] The present study focuses on the post-processed data obtained from the experiment and its application in a DL model to predict unknown patterns of inertial particles in particle-laden turbulent flow with a specified strain rate. To ensure sufficient statistical data for use in the DDM prediction, the experiment for the strained LPT flow was compiled from five repeated video recordings. The designed GRU model applies a time series for each component of displacement, velocity, and acceleration as follows:

- Displacement in the x-direction, 70 373 measured points
- Displacement in the y-direction, 70 373 measured points
- Velocity in the x-direction, 70 373 measured points
- Velocity in the y-direction, 70 373 measured points
- Acceleration in the x-direction, 51 072 measured points
- Acceleration in the y-direction, 51 072 measured points

In the DDM framework, it is crucial to specify the train-test split of the data to train the model and evaluate its predictive performance effectively. The pre-examination of the designed GRU model illustrates that the train-test split 80%–20% is an appropriate setup for computing, error, and accuracy of the model prediction. The focus of the present work is to propose an approach capable of predicting particles in PLT flow. It does not aim to compare different DL models or evaluate varying train-test ratios, as these topics largely pertain to hyperparameter tuning[30] and DL model optimization, which are beyond the scope of this study. The results of the examination are discussed in the results section.

III. DEEP LEARNING DATA-DRIVEN MODEL

This section explores the GRU model architecture and the designed model in this study to forecast the inertial particle's move in PLT flow.

A. GRU architecture

This study proposes a GRU model to forecast the inertial particle move in PLT flow, which is a variant of recurrent neural networks (RNNs) and fundamentally developed after long short-term memory (LSTM) architecture. LSTM and GRU models are designed to address the issue of long-term data dependencies in RNNs, commonly known as the vanishing gradient problem.[47] While LSTM and GRU share similar architectures, GRU operates with fewer gates and parameters, making it computationally more efficient than LSTM.[48] Studies in the literature suggest that the GRU performs comparably to the LSTM while being computationally faster and having a more streamlined design.[49]

A GRU cell consists of three key components: a hidden state, a reset gate, and an update gate. The reset gate determines how much of the previous hidden state should be forgotten, enabling the model to focus on relevant short-term dependencies in the input sequence. Meanwhile, the update gate controls how much of the new hidden state is influenced by the old hidden state, allowing the model to capture long-term dependencies effectively.[48] This unique architecture provides the GRU with two essential capabilities: the reset gate specializes in modeling short-term dependencies, while the update gate excels in retaining long-term dependencies, making it highly effective for sequential data processing tasks.

DL models typically require large datasets to achieve accurate predictions;[50] however, this study introduces a GRU model designed to work effectively with smaller datasets while maintaining accuracy. GRUs offer faster training times and a reduced risk of overfitting on smaller datasets. The gating mechanisms in GRUs facilitate better gradient flow during training, which can result in more stable training processes and faster convergence.

B. GRU model tuning and train-test split

This study employs a GRU model to forecast three sequential variables—displacement, velocity, and acceleration of inertial particles in a strained turbulent flow. The model is trained separately for each variable, with two components: the x- and the y-directions. Since the model performs independent training and testing for each component, it can also be extended to data with a third component (z-direction) by running and testing it accordingly. For each variable, 80% of the data are used for training, while 20% is reserved for testing predictions on unseen data. Given the small dataset, determining the appropriate

training and testing split is crucial. It is common practice to select 60%–80% of the data for training,[51] ensuring sufficient data for the model to learn from.

The data are fed into the GRU network with an input shape defined by the batch size, a sequence length of 30, and a single feature per time step. The GRU processes the input sequence and generates a representation comprising 100 features (units) for each sequence in the batch. This output is then passed to a Dense (fully connected) layer, which takes a 100-dimensional vector for each batch element and reduces it to a single output per sequence, yielding the final prediction for each input. The model's block diagram is illustrated in Fig. 2. The batch size, a hyperparameter that affects both the error rate and training speed, is set to 128 for this model.

The model is implemented in Python using the TensorFlow library[52,53] and is compiled with the adaptive moment estimation (Adam) optimizer,[54] a stochastic gradient descent method that adaptively estimates first- and second-order moments. Adam is computationally efficient, memory-efficient, invariant to diagonal gradient rescaling, and well-suited for handling large datasets or parameter sizes.[51] The dataset was normalized using the MinMaxScaler transformation,[55] which scales the minimum and maximum values to 0 and 1, respectively. Training and inference are conducted on the high-performance computing (HPC) DEEP-DAM system[56] at the Jülich Supercomputing Center, which benefits a modular supercomputer architecture (MSA).[57]

During the training phase, 20% of the training data were reserved as a train-dev set,[51] a cross-validation technique used to fine-tune the model's parameters. The train-dev set involves training the model on a subset of the data and evaluating it on a separate validation (development) set. This method ensures that the model is not assessed on the same data it was trained on, offering a more accurate evaluation of its generalization performance. In cross-validation, the development set varies with each fold, enabling a comprehensive assessment of the model's robustness and reliability across multiple data subsets. Figure 3 displays the convergence diagram of the model for acceleration components. As shown, the training and validation losses decrease from specific points and stabilize at consistent values. The computing time consumed for the model training is 18–21 s.

To assess the model's prediction accuracy, this study utilized the mean absolute error (MAE), root mean squared error (RMSE), and R^2 metrics. These three evaluation metrics are defined by[58]

$$MAE = \frac{1}{N}\sum_{i=1}^{N} |s_{i,a} - s_{i,p}|, \tag{5}$$

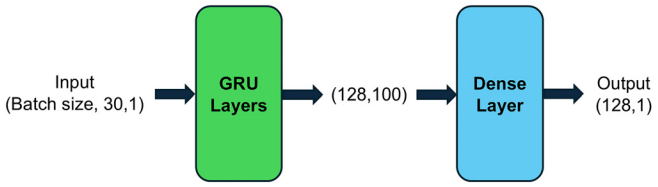

FIG. 2. GRU model: Input shape (batch size, 30, 1), Dense layer output shape (128,1).

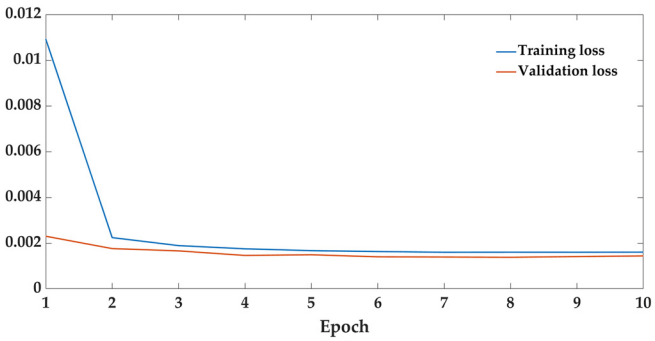

FIG. 3. The DL convergence diagram of the model for acceleration components.

$$RMSE = \sqrt{\frac{1}{N}\sum_{i=1}^{N} (s_{i,a} - s_{i,p})^2}, \tag{6}$$

$$R^2 = 1 - \frac{\sum_{i=1}^{N} (s_{i,a} - s_{i,p})^2}{\sum_{i=1}^{N} (s_{i,a} - s_m)^2}, \tag{7}$$

where $s_{i,a}$ represents the actual measured data, $s_{i,p}$ is the predicted data, s_m is the mean of the actual data, i refers to the corresponding time (or vector array index), and N is the total number of test data points. The MAE provides a straightforward measure of overall error magnitude by averaging the absolute differences between predicted and actual values, treating all errors equally. The RMSE, on the other hand, is more sensitive to large errors because it squares the differences before averaging, giving greater weight to significant deviations or outliers. The R^2 metric evaluates how well the model's predictions align with the observed data.

IV. RESULTS AND DISCUSSION

This section presents and discusses the GRU data-driven model prediction of inertial particle movement in a strained PLT flow.

A. Displacement

Figure 4 illustrates the prediction of inertial particle displacement. The actual data from the measurement are black, the training split data are blue, and the red color represents the prediction. In fact, Fig. 4

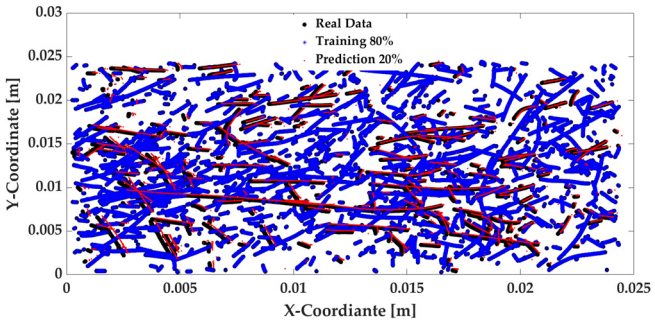

FIG. 4. The prediction of the displacement in plane X–Y of the 2D measurement area. The black-filled circles represent real data, the blue stars indicate training data, and the red points denote predictions.

illustrates the inertial particle displacement among the experiment at the measurement area, which is $24.5 \times 24.5\,\text{mm}^2$. Prior to generating strain deformation, the inertial particles are distributed in the turbulent flow with specific turbulent intensity, as explained in the theory section, and the majority have initial velocity. Thus, the presented data during this measurement are influenced by strain rate in addition to their initial condition.

The GRU model was trained using 80% of the measured data and then used to predict the displacement of the remaining 20% of unseen data, which was tested against the actual measurements. The strength of the GRU model lies in its learning process, where it was trained on a training dataset with varying initial conditions and displaced with the extra influence of the straining deformation, enabling it to extract hidden terms necessary for accurate predictions. While the GRU model is not inherently explainable as a deep learning model, it appears to possess a significant capacity to acquire and utilize physical information to predict unseen data. The red points represent the unseen predicted displacement and exhibit an impressive alignment with the test data (actual measured data in black color). The metric evaluation indicates that the MAE, RMSE, and R^2 are 0.012, 0.057, and 0.95, respectively. These metrics demonstrate the GRU model's strong ability to predict inertial particle movement in this scenario.

Although this study measured the flow over a very short time period, achieving high prediction accuracy with a 20% test split suggests that the model can be effectively applied in similar cases to track specific displacements. Furthermore, the GRU model was trained independently for each directional component, enabling it to separately predict displacement in the x- and y-directions. This capability allows the model to extend its predictions to the third displacement component (z-direction) in applications with all three components.

B. Velocity

In this study, the particle-laden turbulent flow underwent strain deformation. In turbulent flow, it is well addressed that the strain deformation causes extra fluctuation in flow velocity.[59] Figures 5 and 6 display the GRU model prediction for the inertial particle velocity in the x- and y-directions, respectively.

In these figures, the horizontal axis is specified by $S \times t$ to normalize the time duration and have normalized units for comparison. Since, during the experiment, some particles exist from the beginning

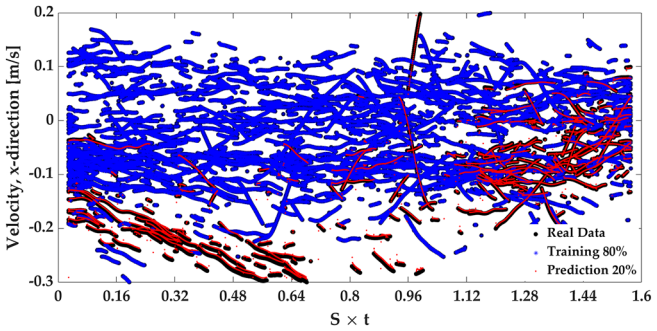

FIG. 5. The prediction of the velocity in the x-direction, S represents the mean strain rate of $8\,\text{s}^{-1}$, and t denotes time in seconds. The black-filled circles represent real data, the blue stars indicate training data, and the red points denote predictions.

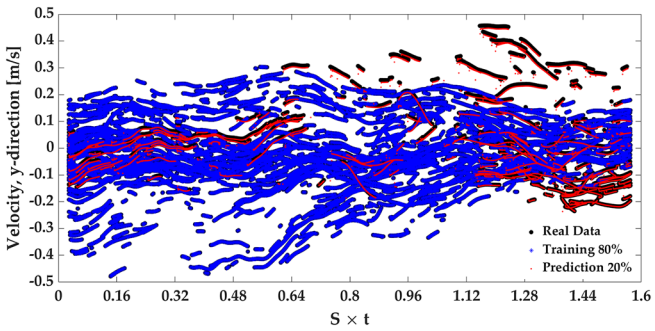

FIG. 6. The prediction of the velocity in the y-direction, S represents the mean strain rate of $8\,\text{s}^{-1}$, and t denotes time in seconds. The black-filled circles represent real data, the blue stars indicate training data, and the red points denote predictions.

in the recording area, some leaving the area, and some entering the area, it is important to capture the velocity of each independent particle. Figure 5 illustrates that the model trained by 80% of the data are able to predict the velocity in the x-direction of the independent inertial particles. The metric measurements show MAE, RMSE, and R^2 are 0.006, 0.026, and 0.97, respectively.

Some inertial particles with higher initial velocities value prior to strain (greater than -0.1 m/s) are more significantly influenced and tend to increase their velocity. In contrast, the majority of inertial particles with velocities in the range of −0.1–0.1 m/s maintain a nearly constant mean velocity with fluctuations. This variation in behavior, driven by different initial conditions, indicates which groups of particles are more affected by strain deformation. Experiments have shown that strain deformation increases the normalized Reynolds stress for inertial particles exhibiting higher fluctuations.[3] Additionally, large-scale effects could be another mechanism that can transfer energy and influence the behavior of inertial particles.

Figure 6 illustrates the GRU model's prediction of inertial particle velocity in the y-direction. Since the strain deformation is generated along the y axis, the velocity of inertial particles in this direction exhibits greater fluctuations compared to the x-direction. Furthermore, for some inertial particles with initial velocities in the range of −0.2–0.2 m/s, the velocity follows a similar pattern throughout the experiment, with fluctuations primarily influenced by strain deformation. However, for another group of inertial particles with initial velocities outside this range, their movement tends to deviate, exhibiting a velocity pattern distinct from the first group. Particles with initial velocities below −0.2 experience a quantitative decrease in velocity, a trend also observed in particles with initial velocities above 0.2.

This indicates that the velocity quantitative of inertial particles with higher velocities are more affected by strain deformation. Additionally, gravity is another factor influencing movement in the y-direction. The inertial force of the particles becomes a dominant factor when its magnitude is significant compared to other forces. As shown in Eq. (4), the gravitational effect increases as the particle mass grows relative to the displaced fluid. It is noteworthy that particles with slightly lower velocities undergo a change in velocity direction (from positive to negative and vice versa), indicating that at a certain moment, the particle reaches a state of rest before speeding in a new direction. The behavior of this group of inertial particles is influenced by various forces, including gravity. In contrast, particles with relatively

higher initial velocities never cross zero and thus do not change direction. This suggests that particles with lower initial velocities are more significantly affected by gravity.

The GRU forecasting model for velocity in the y-direction illustrates considerable alignment with the test data. The measured metrics are MAE = 0.007, RMSE = 0.023, and R^2=0.97. The velocity of the inertial particles in PLT flows carries important properties that can assist in studying these particles—the capability of predicting the velocity, providing a transparent insight into studying PLT flow.

C. Acceleration

In PLT flow, the gravity environment is crucial, and the numerical approach limits prevent its investigation. This study implements the GRU model prediction for PLT data from an experiment in a real-world environment involving gravity effects. The turbulence intensity and strain deformation also influence the inertial particle behavior. Figures 7 and 8 represent the acceleration prediction by the GRU model in the x- and y-directions.

The fluctuations in acceleration in the y-direction are significantly more intense than those in the x-direction, which may be attributed to strain deformation occurring in the y-direction and large-scale influences. Therefore, the predicted data should account for all relevant parameters. Figure 7 illustrates the acceleration of the inertial particle in the x-direction. Visually, the model demonstrates an impressive prediction, with the measured metrics being MAE = 0.012, RMSE = 0.046, and R^2=0.95. The acceleration in the x-direction reveals two main groups of particles. Before the normalized timescale $S \times t \approx 1$, the majority experienced a quantitative loss in acceleration. After this timescale, they maintain a constant mean acceleration with fluctuations. Inertial particles with very small initial acceleration exhibit a change in acceleration direction, momentarily reaching zero. This suggests that inertial particles with higher acceleration are more significantly affected by strain deformation. Notably, inertial particles that experience a sharp reduction in acceleration, which comes near zero bounds, never reach zero acceleration, indicating the presence of a resistance term influencing their behavior.

Figure 8 illustrates the acceleration predictions of inertial particles in the y-direction, demonstrating strong alignment with the test data by MAE = 0.013, RMSE = 0.042, and R^2=0.95. The gravitational environment could influence the y-direction.

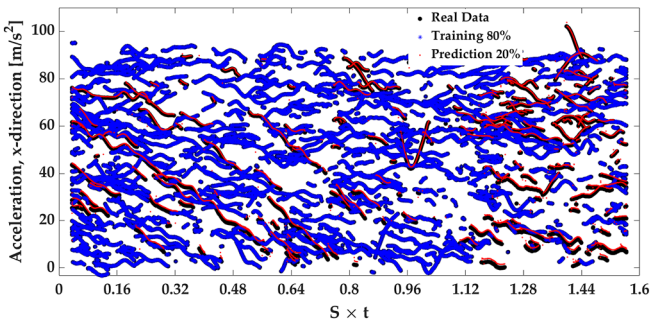

FIG. 7. The prediction of the acceleration in the x-direction, S represents the mean strain rate of 8 s^{-1}, and t denotes time in seconds. The black-filled circles represent real data, the blue stars indicate training data, and the red points denote predictions.

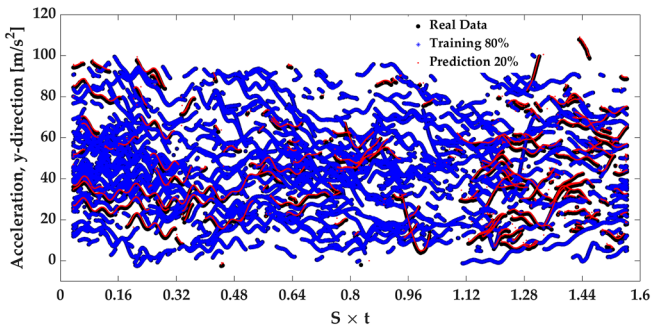

FIG. 8. The prediction of the acceleration in the y-direction, S represents the mean strain rate of 8 s^{-1}, and t denotes time in seconds. The black-filled circles represent real data, the blue stars indicate training data, and the red points denote predictions.

In contrast to the acceleration behavior in the x-direction, the acceleration of inertial particles in the y-direction exhibits distinct patterns. Before the normalized timescale $S \times t \approx 1$ particles with accelerations greater than 50 m/s^2 undergo a sharp reduction in acceleration, while those with lower initial acceleration values follow a consistent pattern with an almost constant mean acceleration and fluctuations. After the normalized timescale $s \times t \approx 1$, particles with initial accelerations below 50 m/s^2 begin to gain acceleration, whereas particles with initial accelerations above this threshold maintain a similar pattern as before.

This observation highlights that, at the onset of strain deformation, particles with higher accelerations are more significantly affected. However, as the strain timescale exceeds the unit scale, the influence primarily shifts to inertial particles with lower initial accelerations. This behavior may be related to the interaction between the fluid phase and the solid particles, as the deformation impacts the fluid flow. Specifically, the strain deformation introduces additional movement and energy into the turbulent flow.

It can be inferred that inertial particles with high acceleration experience damping (resistance) from the fluid flow. Conversely, inertial particles with low acceleration must gain acceleration to align their motion with the fluid flow. The mechanism of this interaction may involve factors such as gravity, the large- and small-scale dynamics of the flow, the size of the particles, the initial conditions of the fluid flow, and the properties of the inertial particles.

Furthermore, suppose the gravity term in Eq. (4) is excluded from the acceleration calculation of the measurement values. In that case, some inertial particles near the zero boundary will exhibit a change in acceleration direction. This indicates that gravity influences these inertial particles more than those with higher initial acceleration.

Looking ahead, incorporating an explanation for DDM could help isolate the effects of gravity on y-direction acceleration and facilitate predictions under non-gravitational conditions. Since Eq. (4) addresses the relationship between acceleration and gravity, it could serve as a tool to include or exclude gravitational influences within the prediction model. Such an analysis could provide deeper insights into the gravitational effects on inertial particles.

D. Physical interpretation in data-driven models

Data-driven models rely solely on data and do not require training based on theoretical or mathematical equations. However, when

DDMs are applied to physical domains, it becomes essential to explore the physical correlations involved. In the context of sequential DL models, as used in this study, training a model solely on the time series of a single variable and accurately forecasting it for unseen periods is a noteworthy achievement. In complex and turbulent systems, one can delve deeper into interpretation by adopting approaches such as determining the influence weights between variables, both directly and reciprocally. Explainable DL is a promising concept that can focus on existing successful DDMs and assess their physical correlations.

However, this physical limitation in interpretation makes it challenging to define the operational range for each DDM.[29] For instance, in the current study, it remains unresolved whether the model can be applied across specific ranges of the Reynolds number (Re) or particle size limits in inertial systems. DDMs can be tailored to specific use cases and applied accordingly, but these limitations still require further investigation. Despite this, DDMs offer valuable insights into studying particle-laden turbulent flows and particle behavior. When combined with PBMs, they help elucidate unmodeled phenomena, aligning with the principles of HAM.

V. CONCLUSION

This study proposes a data-driven modeling (DDM) approach to predict the behavior of inertial particles in particle-laden turbulent (PLT) flows. Experimental data from strain deformation flow with a specified strain rate, and turbulence intensity are employed to train the DDM, forecasting the displacement, velocity, and acceleration of inertial particles based on 2D measurements. Since real-world (3D) measurement data inherently include gravitational effects in PLT flows, numerical studies have not adequately addressed such conditions. DDM leverages data to extract hidden features and predict particle dynamics over unseen timeframes. The Gated Recurrent Unit (GRU) architecture, a variant of Long Short-Term Memory (LSTM) networks, has been enhanced, with each component of the target variables predicted independently.

The DL model is implemented using an 80%–20% train-test split, and a cross-validation technique is applied to fine-tune the model parameters. The results demonstrate significant achievements, highlighting the remarkable capability of DDMs to predict the dynamics of inertial particles in PLT flows. The model's performance is evaluated using three metrics: MAE, RMSE, and R^2.

For displacement prediction, the metrics are measured as MAE = 0.012, RMSE = 0.057, and R^2 = 0.95. Velocity component predictions show MAE values between 0.006 and 0.007, RMSE values between 0.023 and 0.026, and R^2 values between 0.95 and 0.97. For acceleration, the GRU model yields MAE values between 0.012 and 0.013, RMSE values between 0.042 and 0.046, and $R^2 = 0.95$. MAE represents the overall error in predictions, while RMSE captures larger deviations and outliers due to its sensitivity. The measured ranges of MAE and RMSE indicate an acceptable level of error for the proposed forecasting model. Furthermore, R^2 values exceeding 95% demonstrate a strong alignment between the predictions and actual test data.

Understanding the dynamics of inertial particles in PLT flows is crucial, as turbulent flow remains an unsolved physics problem, further complicated by the interaction between particles and the continuous fluid. The proposed approach offers valuable insights into inertial particle behavior in similar use cases and its integration with PBMs. This aligns with the HAM strategy to address unmodeled and unresolved phenomena. Additionally, the authors plan to extend this study by exploring approaches to interpret the physical correlations captured by the prediction model for inertial particles in PLT flows.

ACKNOWLEDGMENTS

The research leading to these results has been conducted in the EuroCC-2 project receiving funding from EU's Horizon 2020 Research and Innovation Framework Programme and European Digital Innovation Hub Iceland (EDIH-IS) (Grant Agreement Nos. 101101903 and 101083762, respectively). The authors thank the technical support of the FreaEnergy team (Energy, AI, and CFD solutions), a startup at Mýrin located in Gróska—innovation and business growth center—in Reykjavik. We thank Ármann Gylfason from Reykjavik University for his technical comments on the experimental data.

AUTHOR DECLARATIONS

Conflict of Interest

The authors have no conflicts to disclose.

Author Contributions

Reza Hassanian: Conceptualization (equal); Data curation (equal); Formal analysis (equal); Methodology (equal); Software (equal); Validation (equal); Visualization (equal); Writing – original draft (equal). **Ásdís Helgadóttir:** Methodology (equal); Writing – review & editing (equal). **Farshad Gharibi:** Formal analysis (equal); Writing – review & editing (equal). **Andrea Beck:** Formal analysis (equal); Writing – review & editing (equal). **Morris Riedel:** Funding acquisition (equal); Methodology (equal); Supervision (equal); Writing – review & editing (equal).

DATA AVAILABILITY

The data that support the findings of this study are available from the corresponding author upon reasonable request.

REFERENCES

[1]H. T. John and L. Lumley, *A First Course in Turbulence* (MIT Press, Boston, MA, 1972).
[2]S. B. Pope, *Turbulent Flows* (Cambridge University Press, London, 2000).
[3]R. Hassanian, A. Helgadottir, L. Bouhlali, and M. Riedel, "An experiment generates a specified mean strained rate turbulent flow: Dynamics of particles," Phys. Fluids **35**, 015124 (2023).
[4]S. Subramaniam and S. Balachandar, *Modeling Approaches and Computational Methods for Particle-Laden Turbulent Flows* (Elsevier (Academic Press), Cambridge, 2022).
[5]A. Beck, P. Ortwein, P. Kopper, N. Krais, D. Kempf, and C. Koch, "Towards high-fidelity erosion prediction: On time-accurate particle tracking in turbomachinery," Int. J. Heat Fluid Flow **79**, 108457 (2019).
[6]J. Wedel, P. Steinmann, M. Štrakl, M. Hriberšek, Y. Cui, and J. Ravnik, "Anatomy matters: The role of the subject-specific respiratory tract on aerosol deposition — a CFD study," Comput. Methods Appl. Mech. Eng. **401**, 115372 (2022).
[7]Z. Chen, J. Lu, C. Zhang *et al.*, "Microclot array elastometry for integrated measurement of thrombus formation and clot biomechanics under fluid shear," Nat. Commun. **10**, 2051 (2019).
[8]A. Ali, G. Abdul-Majeed, and A. Al-Sarkhi, "Review of multiphase flow models in the petroleum engineering: Classifications, simulator types, and applications," Arab. J. Sci. Eng. 1–44 (published online 2024).

[9]G. K. Batchelor, *The Theory of Homogeneous Turbulence* (Cambridge University Press, London, 1982).
[10]S. Elghobashi, "On predicting particle-laden turbulent flows," Appl. Sci. Res. **52**, 309–329 (1994).
[11]M. Alletto and M. Breuer, "One-way, two-way and four-way coupled les predictions of a particle-laden turbulent flow at high mass loading downstream of a confined bluff body," Int. J. Multiph. Flow **45**, 70–90 (2012).
[12]S. Laán, M. Sommerfeld, and J. Kussin, "Experimental studies and modelling of four-way coupling in particle-laden horizontal channel flow," Int. J. Heat Fluid Flow **23**, 647–656 (2002).
[13]J. Kaiser, D. Appel, F. Fritz, S. Adami, and N. Adams, "A multiresolution local-timestepping scheme for particle–laden multiphase flow simulations using a level-set and point-particle approach," Comput. Methods Appl. Mech. Eng. **384**, 113966 (2021).
[14]M. Kuerten, "Point-particle DNS and LES of particle-laden turbulent flow - A state-of-the-art review," Flow. Turbul. Combust. **97**, 689–713 (2016).
[15]S. Patankar, *Numerical Heat Transfer and Fluid Flow* (CRC Press, New York, 1980).
[16]A. Prosperetti, *Computational Methods for Multiphase Flow* (Cambridge University Press, 2007).
[17]P. Kopper, A. Schwarz, S. M. Copplestone, P. Ortwein, S. Staudacher, and A. Beck, "A framework for high-fidelity particle tracking on massively parallel systems," Comput. Phys. Commun. **289**, 108762 (2023).
[18]M. R. Maxey and J. J. Riley, "Equation of motion for a small rigid sphere in a nonuniform flow," Phys. Fluids **26**, 883–889 (1983).
[19]G. I. Taylor, "Diffusion by continuous movements," Proc. London Math. Soc. **s2-20**, 196–212 (1922).
[20]C.-M. Lee, Á. Gylfason, P. Perlekar, and F. Toschi, "Inertial particle acceleration in strained turbulence," J. Fluid Mech. **785**, 31–53 (2015).
[21]P. Wang, J. Li, and X. Zheng, "The effect of gravity on turbulence modulation in particle-laden horizontal open channel flow," Phys. Fluids **33**, 083315 (2021).
[22]S. Elghobashi and G. C. Truesdell, "On the two-way interaction between homogeneous turbulence and dispersed solid particles. I: Turbulence modification," Phys. Fluids A: Fluid Dyn. **5**, 1790–1801 (1993).
[23]G. Tryggvason and J. Lu, "Direct numerical simulations of flows with phase change," Procedia IUTAM 15 **15**, 2–13 (2015).
[24]W. Hwang and J. Eaton, "Turbulence attenuation by small particles in the absence of gravity," Int. J. Multiph. Flow **32**, 1386–1396 (2006).
[25]L. Brandt and F. Coletti, "Particle-laden turbulence: Progress and perspectives," Annu. Rev. Fluid Mech. **54**, 159–189 (2022).
[26]S. Kasmaiee, M. Tadjfar, and S. Kasmaiee, "Machine learning-based optimization of a pitching airfoil performance in dynamic stall conditions using a suction controller," Phys. Fluids **35**, 095121 (2023).
[27]S. Kasmaiee, M. Tadjfar, and S. Kasmaiee, "Optimization of blowing jet performance on wind turbine airfoil under dynamic stall conditions using active machine learning and computational intelligence," Arab. J. Sci. Eng. **49**, 1771–1795 (2024).
[28]S. S. Blakseth, A. Rasheed, T. Kvamsdal, and O. San, "Combining physics-based and data-driven techniques for reliable hybrid analysis and modeling using the corrective source term approach," Appl. Soft Comput. **128**, 109533 (2022).
[29]A. Beck and M. Kurz, "A perspective on machine learning methods in turbulence modeling," GAMM-Mitteilungen **44**, e202100002 (2021).
[30]R. Hassanian, M. Aach, A. Lintermann, A. Helgadóttir, and M. Riedel, "Turbulent flow prediction-simulation: Strained flow with initial isotropic condition using a GRU model trained by an experimental Lagrangian framework, with emphasis on hyperparameter optimization," Fluids **9**, 84 (2024).
[31]R. Hassanian, A. Helgadottir, and M. Riedel, "Deep learning forecasts a strained turbulent flow velocity field in temporal Lagrangian framework: Comparison of LSTM and GRU," Fluids **7**, 344 (2022).
[32]R. Hassanian, H. Myneni, A. Helgadottir, and M. Riedel, "Deciphering the dynamics of distorted turbulent flows: Lagrangian particle tracking and chaos prediction through transformer-based deep learning models," Phys. Fluids **35**, 075118 (2023).
[33]R. Sarma, F. Hübenthal, E. Inanc, and A. Lintermann, "Prediction of turbulent boundary layer flow dynamics with transformers," Mathematics **12**, 2998 (2024).
[34]R. Hassanian, M. Riedel, and L. Bouhlali, "The capability of recurrent neural networks to predict turbulence flow via spatiotemporal features," in *2022 IEEE 10th Jubilee International Conference on Computational Cybernetics and Cyber-Medical Systems (ICCC)* (IEEE, 2022), pp. 000335–000338.
[35]J. Hu, Z. Lu, and Y. Yang, "Improving prediction of preferential concentration in particle-laden turbulence using the neural-network interpolation," Phys. Rev. Fluids **9**, 034606 (2024).
[36]T. Maurel-Oujia, S. S. Jain, K. Matsuda, K. Schneider, J. R. West, and K. Maeda, "Neural network models for preferential concentration of particles in two-dimensional turbulence," Theor. Comput. Fluid Dyn. **38**, 917–935 (2024).
[37]A. Haghshenas, S. Hedayatpour, and R. Groll, "Prediction of particle-laden pipe flows using deep neural network models," Phys. Fluids **35**, 083320 (2023).
[38]Z. Yang, K. Li, and M. Barigou, "Experimentally trained hybrid machine learning algorithm for predicting turbulent particle-laden flows in pipes," Phys. Fluids **35**, 113309 (2023).
[39]J. Boussinesq, *Application des potentiels à l'étude de l'équilibre et du mouvement des solides élastiques, principalement au calcul des déformations et des pressions que produisent, dans les solides, des efforts quelquonques exercés sur une petite partie de leur surface ou de leur intérieur : mémoire suivi de notes étendues sur divers points de physique mathématique et d'analyse* (Gauthier-Villars, Paris, 1885), Chap. 8.
[40]A. Basset, *A Treatise on Hydrodynamics*, Vol. *2*, Ch. 21 (Bell and Co. (Also Dover Publications, Inc., New York, 1961), Deighton, Cambridge, 1888).
[41]P. G. Saffman, "The lift on a small sphere in a slow shear flow," J. Fluid Mech. **22**, 385–400 (1965).
[42]P. G. Saffman, "The lift on a small sphere in a slow shear flow - Corrigendum," J. Fluid Mech. **31**, 624 (1968).
[43]J. B. McLaughlin, "Inertial migration of a small sphere in linear shear flows," J. Fluid Mech. **224**, 261–274 (1991).
[44]P. Shi and R. Rzehak, "Lift forces on solid spherical particles in unbounded flows," Chem. Eng. Sci. **208**, 115145 (2019).
[45]W. Gao, P. Shi, M. Parsani, and P. Costa, "On the relevance of lift force modelling in turbulent wall flows with small inertial particles," J. Fluid Mech. **988**, A47 (2024).
[46]R. Hassanian and M. Riedel, "Leading-edge erosion and floating particles: Stagnation point simulation in particle-laden turbulent flow via Lagrangian particle tracking," Machines **11**, 566 (2023).
[47]S. Hochreiter and J. Schmidhuber, "Long short-term memory," Neural Comput. **9**, 1735–1780 (1997).
[48]K. Cho, B. van Merriënboer, C. Gulcehre, D. Bahdanau, F. Bougares, H. Schwenk, Y. Bengio, and W. Daelemans, "Learning phrase representations using RNN encoder–decoder for statistical machine translation," in *Proceedings of the 2014 Conference on Empirical Methods in Natural Language Processing (EMNLP)*, edited by A. Moschitti, B. Pang, and W. Daelemans (Association for Computational Linguistics, Doha, Qatar, 2014), pp. 1724–1734.
[49]J. Chung, C. Gulcehre, K. Cho, and Y. Bengio, "Empirical evaluation of gated recurrent neural networks on sequence modeling," in *NIPS 2014 Workshop on Deep Learning, December 2014* (NIPS, 2014).
[50]L. Alzubaidi, J. Bai, A. Al-Sabaawi, J. Santamaría, A. Albahri, B. Al-dabbagh, M. Fadhel, M. Manoufali, J. Zhang, A. Al-Timemy, Y. Duan, A. Abdullah, L. Farhan, Y. Lu, A. Gupta, F. Albu, A. Abbosh, and Y. Gu, "A survey on deep learning tools dealing with data scarcity: Definitions, challenges, solutions, tips, and applications," J. Big Data **10**, 46 (2023).
[51]A. Géron, *Hands-On Machine Learning with Scikit-Learn, Keras, and TensorFlow: Concepts, Tools, and Techniques to Build Intelligent Systems* (O'Reilly Media, Sebastopol, 2019).
[52]M. Abadi, A. Agarwal, P. Barham, E. Brevdo, Z. Chen, C. Citro, G. S. Corrado, A. Davis, J. Dean, M. Devin *et al.*, "Tensorflow: Large-scale machine learning on heterogeneous distributed systems," arXiv:1603.04467 (2016).
[53]M. Abadi, P. Barham, J. Chen, Z. Chen, A. Davis, J. Dean, M. Devin, S. Ghemawat, G. Irving, M. Isard *et al.*, "Tensorflow: A system for large-scale machine learning," arXiv:1605.08695 (2016).
[54]D. P. Kingma and J. Ba, "Adam: A method for stochastic optimization," arXiv:1412.6980 (2017).
[55]O. Kramer and O. Kramer, "Scikit-learn," in *Machine Learning for Evolution Strategies* (Springer, 2016), pp. 45–53.
[56]Research Centre Jülich, *Deep Learning Prototype Systems: Deep Systems* (Research Centre Jülich, n.d.).

[57]M. Riedel, R. Sedona, C. Barakat, P. Einarsson, R. Hassanian, G. Cavallaro, M. Book, H. Neukirchen, and A. Lintermann, *Practice and Experience in Using Parallel and Scalable Machine Learning with Heterogenous Modular Supercomputing Architectures* (IEEE, 2021).

[58]C. Gu and H. Li, "Review on deep learning research and applications in wind and wave energy," Energies **15**, 1510 (2022).

[59]P. A. Davidson, *Turbulence: An Introduction for Scientists and Engineers* (Oxford University Press, London, 2004).